# Structural, thermodynamic, thermal, and electron transport properties of single-crystalline $LaPt_2Si_2$

M. Falkowski,[1,2,*] P. Doležal,[1] A. V. Andreev,[2] E. Duverger-Nédellec,[1] and L. Havela[1]
[1]*Department of Condensed Matter Physics, Faculty of Mathematics and Physics, Charles University, Ke Karlovu 5, 12116 Prague, Czech Republic*
[2]*Institute of Physics of the Czech Academy of Sciences, Na Slovance 2, 18221 Prague, Czech Republic*

(Received 15 March 2019; revised manuscript received 2 August 2019; published 20 August 2019)

$LaPt_2Si_2$ in a single-crystalline form was subjected to structure, thermodynamic, thermal, and electron transport studies with a special emphasis on the structure phase transition appearing at $T = 85$ K. X-ray diffraction proves the noncentrosymmetric tetragonal structure of $CaBe_2Ge_2$-type (space group $P4/nmm$). The transition manifests as a small step of opposite sign in both lattice parameters, leaving almost no volume change. $c$ decreases and $a$ increases in the low-$T$ phase, but the change of the $c/a$ ratio does not exceed 0.1%. Additional periodicity, related to the supposed charge density wave (CDW) state, can be related to satellites corresponding to the wave vector $q \approx (0.36, 0, 0)$, which start to grow with temperature decreasing below 175 K and almost vanish (or relocate from the investigated $ab$ plane) below the 85 K transition. Electrical resistivity reveals that the 85 K transition is hysteretic in temperature, with the difference between heating and cooling being almost 10 K, proving the first-order type of the transition. The transition dramatically enhances resistivity in the low-$T$ state, pointing to a formation of a pseudogap. This, however, does allow a superconducting state, arising below $T_c = 1.6$ K. The temperature dependence up upper critical field is not compatible with the weak coupling BCS theory. Strong anisotropy of electronic structure and its dramatic changes at the structure transition are manifest also in thermal expansion and thermoelectric power. The Sommerfeld coefficient $\gamma = 7.8$ mJ mol$^{-1}$ K$^{-2}$ and Debye temperature of 205 K could be derived at low temperatures, but the specific heat has a strongly non-Debye like $T$ dependence, which can be ascribed to a low-energy Einstein mode.

DOI: 10.1103/PhysRevB.100.064103

## I. INTRODUCTION

Single-crystalline $LaPt_2Si_2$ was reported to be a charge density wave (CDW) system, most likely exhibiting a first-order phase transition at $T_{CDW} = 85$ K, or even a crystal structure modification, and becomes superconducting at $T_c = 1.79$ K [1]. The coexistence of the CDW state and superconductivity, two entirely different cooperative phenomena, is rare, hence this case has been interesting especially from the point of view of physics of low-dimensional systems [2–4]. The formation of the CDW commonly happens in metallic systems with low-dimensional [one- (1D) or two-dimensional (2D)] character of their crystal structure, where a large anisotropy in the Fermi surface topology leads to the low-$T$ structural instability accompanied by a periodic lattice distortion [5–7]. However, three-dimensional (3D) materials that display CDW are particularly interesting. Only a few examples can be found in the literature of 3D materials exhibiting the CDW behavior, examples being $LaAgSb_2$ [8–10], $Lu_5Ir_4Si_{10}$ [11,12], $Lu_2Ir_3Si_5$ [13,14], $Lu_5Rh_4Si_{10}$ [15], or ternary rare earth nickel carbides, $RNiC_2$ ($R$ = Pr, Nd, Sm, Gd, Tb), which manifest an interplay of CDW and magnetic order [16–19]. A sequence of CDW transitions takes place also for pure uranium metal as a 3D system [20]. It is interesting that its superconductivity was found mutually exclusive with fully developed CDW state [21].

In the case of $LaPt_2Si_2$, the "dimensionality" issue does not seem to be fully clear. Based on the *ab initio* density functional theory band structure and phonon calculations [22,23], it was found that the Fermi surface in $LaPt_2Si_2$ has a 2D nature and the CDW state arises from the electron-phonon coupling with a quasinesting feature of the Fermi surface. The density of states (DOS) at the Fermi level mainly consists of Pt1-$d$ orbitals, while the Pt2-$d$ orbitals contribute much less [22], and CDW and superconductivity coexist in the (Si2-Pt1-Si2) layer [23]. On the other hand, recent experimental results indicate that an energy gap opened at the Fermi surface due to the CDW transition could have anisotropic nature and thus a 3D character [1]. This issue still requires further investigations.

As part of the effort to better understand the structural and transport properties of $LaPt_2Si_2$ and the underlying mechanisms associated with the CDW features in bulk properties, we used a $LaPt_2Si_2$ single crystal for in-depth study of the crystal structure in a wide $T$ range, as well as for the measurements of thermal and electron transport properties. In the present paper, results of measurements of thermoelectric power and thermal conductivity of the single-crystalline $LaPt_2Si_2$ compound are described. No detailed crystal structure investigation of this compound has been reported so far. The room-temperature XRD measurements of single-crystalline sample by Gupta *et al.* [1] have confirmed a tetragonal structure of $CaBe_2Ge_2$-type, however, no low-$T$ crystallographic information is

*On leave from the Institute of Molecular Physics, Polish Academy of Sciences, Poznań, Poland; falkowski@ifmpan.poznan.pl

 

provided. A structure study of the polycrystalline material revealed a structural transition from high-$T$ tetragonal to low-$T$ orthorhombic symmetry at $T^* = 112$ K, showing a clear splitting of the $(220)_T$ reflection peak into two subpeaks $(400)_O$ and $(040)_O$ with nearly equal intensity below $T = 100$ K [24]. In a recent investigation of the physical properties of single-crystalline $LaPt_2Si_2$ [1] the authors suggest that also in this case the formation of the CDW state could be associated with the structural phase transition. Nonetheless, the nature of the CDW transition in this compound is still not fully clarified. Because of the importance of the structure features we studied the crystal structure in a wide $T$ range for a carefully prepared sample with well-defined composition.

## II. EXPERIMENTAL DETAILS

A single crystal of $LaPt_2Si_2$ was grown by the modified Czochralski method in a triarc furnace on a copper water-cooled bottom under an argon protective atmosphere. Initial 8-g ingot was prepared from high-purity elements (99.9% La, 99.99% Pt, 99.999% Si) mixed in stoichiometric ratio with 1% excess of La. Tungsten rod was used as a seed, pulling speed was 15 mm/hour. The single-crystalline state of the pulled cylinder was confirmed by the backscattering Laue method [see inset (a) in Fig. 1]. The correct structure and composition of the crystal were confirmed by x-ray diffraction (XRD) and x-ray energy dispersive microanalysis (EDX) experiments. EDX analysis confirmed the single phase character [see inset (b) in Fig. 1] yielding a ratio La : Pt : Si $\simeq$ 19.8 at.% : 40.1 at.% : 40.1 at.% which is in very good agreement with the ideal ratio of the elements. The x-ray powder diffraction was performed on Siemens D500 theta-theta diffractometer equipped with a 1D Mythen 1 K position sensitive detector in the Bragg-Brentano geometry with Cu $K_{\alpha 1,2}$ radiation. Cu $K_\beta$ line was suppressed by a Ni filter. The crystallographic characterization was carried out on a crushed piece of a single crystal at a various temperatures between $T = 5$ and 300 K. We used the setup described in Ref. [25]. Collected data were refined using the FULLPROF program [26]. In addition, reciprocal space maps of selected reflections were measured and the radial scans were obtained by an integration in a rocking direction, which allows us to observe better the $2\theta$ profile of the diffraction lines. Changes in the shape of diffraction profile are crucial in proximity of the structural transition, where the splitting of the peaks is usually very small. The sample was placed in the cryostat (ColdEdge) in helium atmosphere to achieve good thermal contact with the "cold finger," allowing measurements down to 5 K. The stabilization of temperature during the XRD measurements was better than 0.1 K.

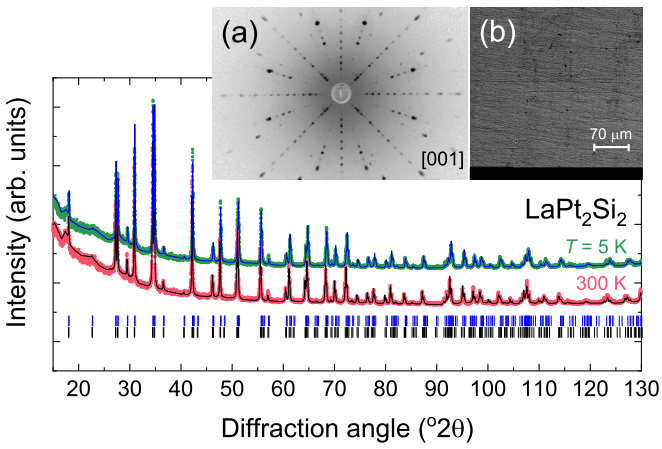


FIG. 1. XRD powder patterns of $LaPt_2Si_2$ collected at $T = 5$ and 300 K refined using the $CaBe_2Ge_2$-type structure, space group $P4/nmm$ (blue and black lines, respectively). The peak positions are indicated by the vertical bars bellow the data. Inset (a) shows the Laue diffraction pattern of $LaPt_2Si_2$ single crystal with a view along the [001] axis. Inset (b) shows the SEM micrograph obtained from the surface of single-crystalline $LaPt_2Si_2$ used for the EDX analysis.

From the obtained single crystal ingot, we were able to prepare only one large rectangular bar-shaped sample appropriate for the TTO (Thermal Transport Option) measurements, which was cut from the ingot using a wire saw with the long dimension parallel to the [110] axis. The sample dimensions were $1.6 \times 1.2 \times 4.2$ mm$^3$ for the heat and electron current flow $j \parallel$ [110] axis. In the case of measurements taken along the [001] axis, we shortened the mentioned bar-shaped sample to dimensions 1.6 mm along [110] axis, 1.2 mm along [001] axis, and 2.5 mm along [110] axis, and the electrodes were attached in a configuration concentrating the heat and electron current flow $j \parallel$ [001] axis.

The measurements of all thermodynamic and transport properties presented in this paper were carried out on a physical property measurement system PPMS apparatus from *Quantum Design*, San Diego. Thermoelectric power and thermal conductivity measurements were performed simultaneously in the $T$ range between 2 and 300 K. The experiment was performed at slow cooling/warming continuous mode (0.2 K/min) by applying a direct heat-pulse with steady state heat-flow technique maintaining a high vacuum of $10^{-3}$ Pa. Electrical resistivity measurements were conducted in a four-point probe arrangement with gold conducting wires established by spot welding. The [110] and [001] axis resistivity was measured simultaneously on two different samples, cut from the piece previously used in the TTO experiment. If magnetic field was applied, the field direction was perpendicular to the direction of electrical current.

## III. RESULTS AND DISCUSSION

### A. X-ray characterization

All diffraction powder patterns collected in the $T$ range 5–300 K have been successfully refined within the tetragonal $CaBe_2Ge_2$ model (with space group $P4/nmm$), showing that the tetragonal symmetry in single-crystalline $LaPt_2Si_2$ is preserved down to low temperatures. No traces of any parasitic phases are detected. In Fig. 1, we show the obtained XRD patterns obtained at room temperature (red symbols) and $T = 5$ K (green symbols). The refined lattice parameters obtained at room temperature [$a = 4.2846(4)$ Å and $c = 9.8280(9)$ Å] and the volume of the unit cell $V_{\text{cell}} = 180.42(4)$ Å$^3$ agree very well with the previous results for a single-crystalline sample [1]. The temperature dependence of the lattice parameters $a$

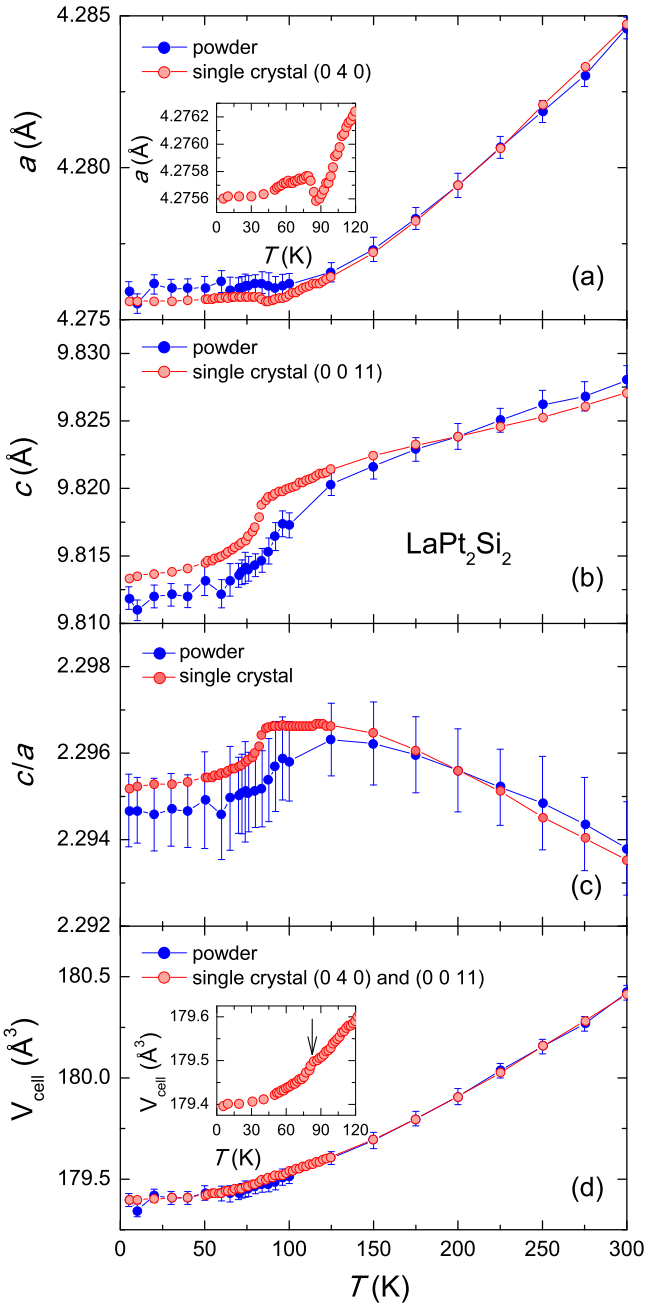


FIG. 2. Temperature dependence of the lattice parameters $a$ and $c$, the $c/a$ ratio, and the unit cell volume of $LaPt_2Si_2$ determined for powder and single crystal samples. The insets emphasize the anomalous behavior of $a$ and the volume of the tetragonal unit cell in the vicinity of 85 K. The horizontal error bars for the uncertainty of temperature at each point are not shown in the graph, because they are smaller than the experimental data points.

and $c$, the $c/a$ ratio, and unit cell volume are presented in Figs. 2(a)–2(d).

The temperature dependencies exhibit an anomaly in the vicinity of $T = 85$ K. Suspecting a CDW transition, we call henceforth the temperature $T_{CDW}$. During cooling the lattice parameters show a decreasing trend, i.e., regular thermal contraction. One can notice that the linear thermal expansion at high temperatures is anisotropic, with the higher expansion along the $a$ axis, with the coefficient $\alpha_a = 13 \times 10^{-6}\,\mathrm{K}^{-1}$ by a factor of 4 higher than $\alpha_c = 3.4 \times 10^{-6}\,\mathrm{K}^{-1}$. This anisotropy, which is regularly correlated with an elastic anisotropy, reflects different bonding conditions within the basal plane and along the $c$-axis, respectively. It would be interesting to compare with other isostructural compounds to see whether the anisotropy is a generic feature of the structure type. As the anisotropy of thermal expansion $\alpha_i$ reflects (both theoretically and experimentally) the anisotropy of linear compressibility $k_i$, following the relation: $\alpha_i = k_i \Gamma_\Theta C_V / V$, with $\Gamma_\Theta$ standing for the Grüneisen parameter, $C_V$ is the molar specific heat at constant volume and $V$ the molar volume [27], we can assume that the $c$ direction would be much harder in terms of linear compressibility under hydrostatic pressure. The total volume thermal expansion $\alpha_V = 2\alpha_a + \alpha_c \approx 30 \times 10^{-6}\,\mathrm{K}^{-1}$ has a rather normal value. Cooling below 200 K, both parameters tend to a usual saturation. However, in the vicinity of 85 K, the $c$ parameter exhibits a sudden drop, while $a$ has a negligible increase [see inset in the panel (a)]. As the two effects largely compensate, the unit cell volume exhibits only an anomalous hump, clearly visible in the inset at the panel (d). The $c/a$ ratio drops by less than 0.1% below the transition. All effects are relatively small when comparing with their impact on transport properties described below, therefore the modulation of the structure below $T_{CDW}$ is expected to explain the anomaly. The x-ray powder patterns did not give any evidence of satellite diffraction peaks or splitting of the $hk0$ peaks. In order to check for a small possible splitting of $hk0$ diffraction peaks (indicating a putative orthorhombic distortion) at $T^* = 112$ K, as well as to indicate a modulated structure below $T^*$ (previously indicated for a polycrystalline sample [24]) we carried out also measurements of reciprocal space maps on a rectangular single-crystalline sample for the selected diffraction peaks and their $k$-space neighborhood. In particular, we took the (0 4 0), (0 0 11), and (1 5 0) reflections. This experiment was performed by using the same diffractometer, as used for the powder (crushed) sample, but the sample holder was equipped with a piezorotator for the alignment of the single crystal. Lattice parameters determined in such way have a larger uncertainty of absolute values, but have a higher precision. We tried to get more details using integration of intensity of selected diffraction peaks in a rocking direction [see Figs. 3(a)–3(c)].

Figure 3 shows the temperature variations of the (0 4 0) and (0 0 11) diffraction intensities, which reflect the development of $a$ and $c$. In agreement with the powder data, a subtle structure change is noticeable at both lattice parameters. In particular we see the shift of the (0 0 11) peak, which confirms the observation coming from the Rietveld analysis [see Fig. 2(b)]. Also the (0 4 0) diffraction is influenced by the structure change. We can clearly see the small increase of $a$ at the same temperature as the anomaly in $c$ appears. The unit cell volume slightly decreases around transition. We also explored the (2 4 0) and (1 5 0) peaks, which would be split in case of an orthorhombic distortion. Figure 3(c) captures the (1 5 0) peak. One can see a change of the shape profile, but no splitting. In Fig. 3(d), we can observed the change of full width at half maximum (FWHM). The changes of FWHM for (0 4 0) and (1 5 0) are in a qualitative agreement. A small change is also visible for the case of (0 0 11).

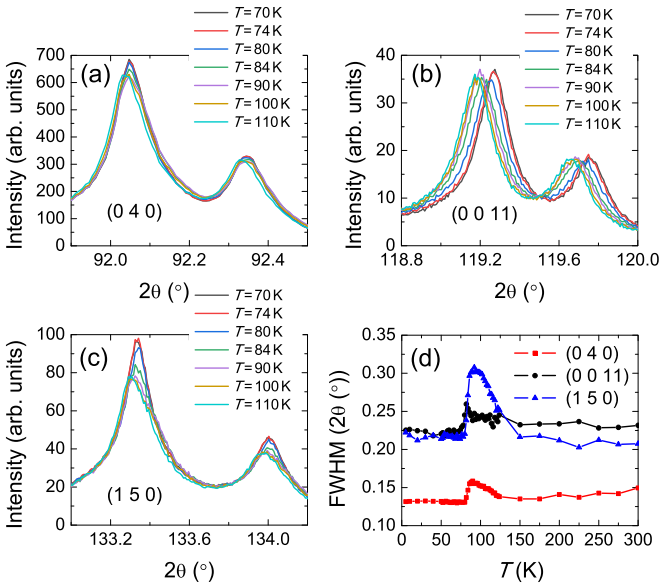


FIG. 3. (a)–(c) show the radial scans obtained by integration in a rocking direction for (0 4 0), (0 0 11), and (1 5 0) diffraction peaks, respectively. (d) shows the temperature dependence of full width at half maximum for measured radial scans. The estimated error bars of FWHM of the diffraction peaks have similar size for all temperatures, and are estimated as $\pm 0.01^\circ$ for (0 4 0), $\pm 0.01^\circ$ for (0 0 11), and $\pm 0.02^\circ$ for (1 5 0).

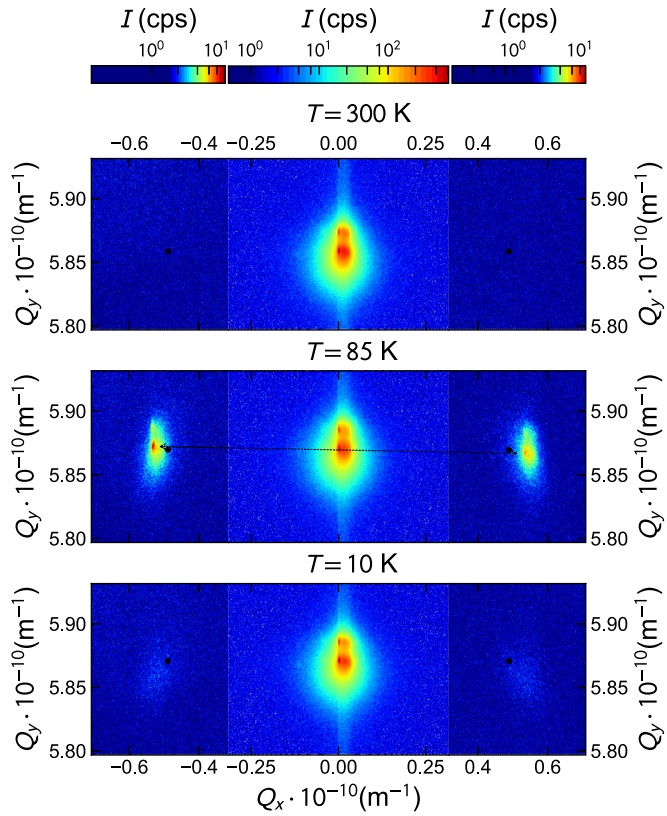


FIG. 4. Reciprocal space map of (0 4 0) diffraction at $T = 300$, 85, and 10 K. The scattering plane corresponds to the basal plane. The black point shows the position of $q = (1/3, 0, 0)$.

Figure 4 shows the temperature dependence of a reciprocal map around (0 4 0), where the scattering plane corresponds to the *ab* plane of the unit cell. We can clearly observe two satellites at $T = 85$ K, which appear almost at the $Q_x$ direction. In the direction $Q_y$ no satellites were observed. The observed satellites are in a qualitative agreement with the selected-area used for electron diffraction analysis [24]. Similar situation was found also for the (2 4 0) diffraction. The temperature dependence of integrated intensity and position of satellites in the $Q_x$ and $Q_y$ directions is shown in Fig. 5. The formation of satellites, indicating structural modulation, is not directly connected with the anomaly of lattice parameters at 85 K, but it develops gradually below 175 K. The intensity saturates around 100 K and decreases fast below 85 K. Below 60 K, it remains weak and approximately constant. The intensity variations are connected with the shift of the satellites, see Figs. 5(b) and 5(c). The $h$ and $k$ positions could be determined only in the range 85−120 K, where the intensity is sufficient and well localized in the $k$ space. The intensity above 120 K corresponds rather to a diffuse scattering than to clear peaks. Figure 3(d) indicates that FWHM of main diffraction peaks is correlated with the intensity of the satellites. The above mentioned observation is clear evidence of lowering of the tetragonal symmetry and points to a CDW state at low temperatures.

With present experimental setup, which does not allow manipulation of the sample position at low temperatures, we cannot rule out the possibility that the decrease of the satellites intensity is due to their displacement out of the *ab* plane below 85 K, or change of modulation vector. The complete reciprocal space study requires a single crystal diffractometer with low-$T$ capabilities. Such experiment will also determine more precisely the position of satellites. In Fig. 5(b), we show the absolute values of the $h$ coordinates of the $q$ and $-q$ vectors. The value should be the same if we assume a periodic modulation. The actual observed values slightly differ, and the difference is at the border of an experimental error if we assume a small mosaicity of the sample. The $h$ value is close to 0.36 which is quite far from the proposed value $q = (1/3, 0, 0)$ [24] (black points in Fig. 4), therefore the modulation would be incommensurate.

### B. Specific heat

The temperature dependence of specific heat $C_p(T)$ of $LaPt_2Si_2$ measured during cooling and warming process are shown in Fig. 6. The resulting temperature dependence and overall absolute values of specific heat are similar to those reported in Ref. [1]. A well-defined anomaly in $C_p(T)$ visible at $T = 85$ K is most likely related to the lattice anomalies manifested in structure studies. On the contrary to previous results given by Gupta *et al.*, [1] in our case a small but visible hump in $C_p(T)$ was also detected for cooling mode—see inset (a) in Fig. 6. One has to realize that the semiadiabatic method used in the PPMS equipment for specific heat measurement relies on analysis of $T$ relaxation after a heating pulse even in the cooling regime, so the difference can be on the "technical" level, i.e., the size of particular sample and heating power in each pulse.

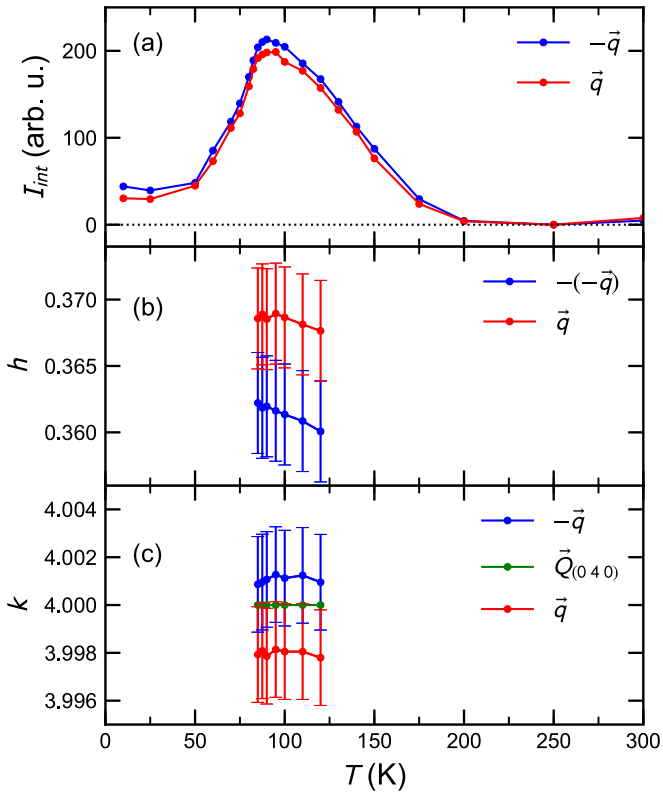


FIG. 5. (a) Temperature dependence of integrated intensity of the satellites. [(b) and (c)] Temperature dependence of $h$ and $k$ position of satellites in the basal plane.

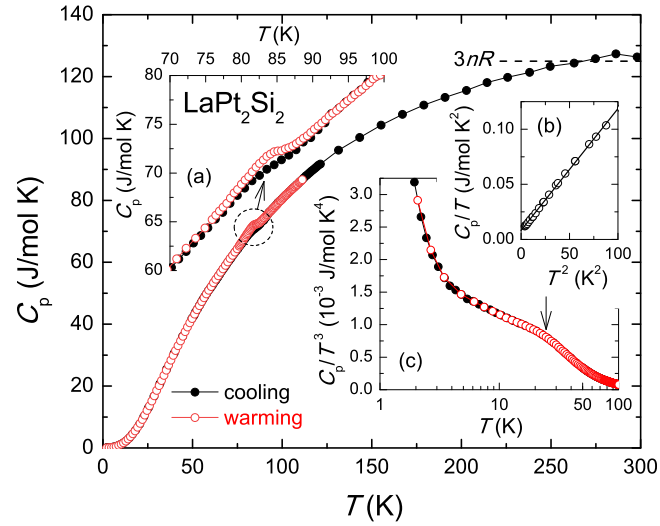


FIG. 6. Temperature dependence of the specific heat $C_p(T)$ of $LaPt_2Si_2$ measured on subsequent at cooling and warming cycles. Inset (a) highlights the presence of thermal irreversibility effect around 85 K and indicates the first-order phase transition. Inset (b) shows the low-$T$ part as $C_p(T)/T$ vs $T^2$ and fit from the Debye temperature and electronic specific heat coefficient are evaluated. Inset (c) illustrates the temperature dependence of the ratio $C_p(T)/T^3$ where the local hump seen at 25 K might indicate the involvement of Einstein modes in the specific heat.

Below $T = 10$ K, a linear extrapolation of the $C_p(T)/T$ versus $T^2$ data to $T \to 0$ by using the formula $C_p(T)/T = \gamma + \beta T^2$ [see inset (b) in Fig. 6] gives the Sommerfeld coefficient $\gamma = 7.8$ mJ mol$^{-1}$ K$^{-2}$ and the $\beta$ parameter equal to $11.2 \times 10^{-4}$ J mol$^{-1}$ K$^{-4}$, which is related to the Debye temperature through the expression $\theta_D = \sqrt[3]{\frac{12\pi^4 n\mathrm{R}}{5\beta}}$ with the gas constant R = 8.31 J mol$^{-1}$ K$^{-1}$ and $n = 5$ for the number of atoms per unit cell. The value of the Debye temperature extracted from this low-$T$ fit is 205 K. At $T = 300$ K, the $C_p$ data reach a value of 126.3 J mol$^{-1}$ K$^{-1}$ and fairly agree with the classical Dulong-Petit value of 124.7 J mol$^{-1}$ K$^{-1}$ enhanced by the electronic term $\gamma T = 2.3$ J mol$^{-1}$ K$^{-1}$. The description in the intermediate $T$ range is, however, less satisfactory.

In the inset (c) of Fig. 6, we plotted the temperature dependence of the ratio $C_p(T)/T^3$ for $LaPt_2Si_2$, a representation that is often used to assess the presence of low-frequency phonon excitations, so-called Einstein modes in the specific heat [28]. In that way, one can indirectly indicate the presence of optical modes by plotting $C_p(T)/T^3$ versus $T$, which should reveal a low-$T$ maximum caused by the excess low-frequency vibrations, giving rise to deviation of the specific heat from the Debye model. The used semilogarithmic scale in the inset (c) in Fig. 6 helps to stress in more details the presence of the hump in the ratio $C_p(T)/T^3$. As the La ions are nonmagnetic ($4f^0$), possibilities related to $4f$-electron excitations are ruled out, therefore no Schottky contribution due to the crystal electric field splitting is present. That is why the visible flat hump at $T \approx 25$ K in $C_p(T)/T^3$ could suggests the presence of the low-$T$ Einstein contribution and also the temperature where the deviation from a pure Debye description of the specific heat becomes conspicuous.

As next, we tried to describe the specific heat quantitatively below and above the anomaly at $T = 85$ K by using the standard Debye model and combined Debye and Einstein models. The Debye specific heat is given by the equation [29]

$$C_D(T) = 9n\mathrm{R}\left(\frac{T}{\theta_D}\right)^3 \int_0^{\theta_D/T} \frac{x^4 e^x dx}{(e^x - 1)^2}, \qquad (1)$$

where $x = \theta_D/T$. However, as can be seen from Fig. 7, this model provides a realistic description of $C_p(T)/T$ versus $T$ only in the range 95–300 K. The parameters $\gamma^{HT} = 30$ mJ mol$^{-1}$ K$^{-2}$ and $\theta_D^{HT} = 328$ K are rather different than those obtained in the low-$T$ estimate given above. The *HT* and *LT* indexes refer to the high- and low-$T$ area, respectively. In particular the $\gamma$ value higher by a factor of 4 and much stiffer lattice deduced from the higher Debye temperature suggest that the density of states at the Fermi level is reduced by a gapping in the low-$T$ state, while the lattice below $T_{\mathrm{CDW}}$ is softer. On the other side, when we start from the low-$T$ end, the applicability of the Debye law is limited only up to 20 K, using the parameters $\gamma^{LT} = 7.8$ mJ mol$^{-1}$ K$^{-2}$ and $\theta_D^{LT} = 217$ K obtained from the $C_p/T$ versus $T^2$ plot. This may be related to a low-energy Einstein mode, suggested above. Therefore, we tentatively replaced some Debye modes by Einstein modes [29]

$$C_E(T) = 3n\mathrm{R}\left(\frac{\theta_E}{T}\right)^2 \frac{e^{\theta_E/T}}{(e^{\theta_E/T} - 1)^2}, \qquad (2)$$

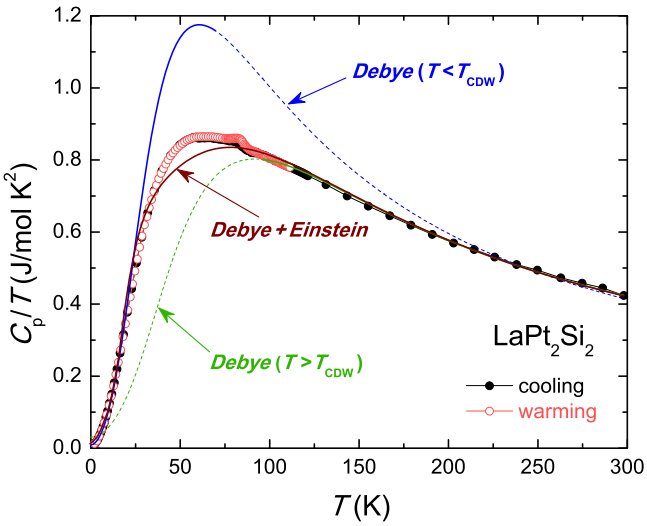


FIG. 7. The temperature dependence of the ratio $C_p/T$ of $LaPt_2Si_2$ single crystal with corresponding fit lines by using the Debye approximation for temperature both below and above the anomaly at $T = 85$ K, and also combination of Debye and Einstein models as discussed in the text.

where $x_E = \theta_E/T$ and $\theta_E$ is the Einstein temperature, in order to find out how the Einstein-type oscillators (representing low-lying optical phonons) can affect the specific heat of $LaPt_2Si_2$. Adding 3 or 6 Einstein vibration modes (3 per atom) with $\theta_E \approx 100$ K and subtraction the same number of Debye modes improved the fit only slightly. The best result, shown in Fig. 7, was achieved for a combination of 25% of Einstein and 75% of Debye modes using the parameters $\gamma = 12$ mJ mol$^{-1}$ K$^{-2}$, $\theta_D = 395$ K, and $\theta_E = 93$ K, which describe the measured data in the whole $T$ range except the interval 40–85 K. The complex temperature variations of the specific heat, which cannot be described by a simple model in the whole low- and high-$T$ range, does not allow to quantify a possible step in $\gamma$ at $T = 85$ K.

### C. Electrical resistivity

Figure 8 displays the temperature dependence of the electrical resistivity $\rho(T)$ of $LaPt_2Si_2$ measured with current $j$ along [110] and [001] axis both for cooling and warming regime. The room temperature values of 66 $\mu\Omega$cm for the [110] axis and 148 $\mu\Omega$cm for the [001] axis are comparable with those previously reported for a single-crystal material [1]. Above the anomaly ($T > T_{CDW}$) $\rho$(T) of $LaPt_2Si_2$ (for both crystallographic directions) can be well described in the framework of the Bloch-Grüneisen-Mott (BGM) equation, usually applicable to the conventional metals [30]

$$\rho(T) = \rho_0 + \frac{4A_0}{\theta_R}\left(\frac{T}{\theta_R}\right)^5 \times \int_0^{\theta_R/T} \frac{x^5 dx}{(e^x - 1)(1 - e^{-x})} - KT^3, \qquad (3)$$

where $\rho_0$ represents the contribution to resistivity from electron-impurity scattering, the second term describes the electron-phonon contribution to the total resistivity in which

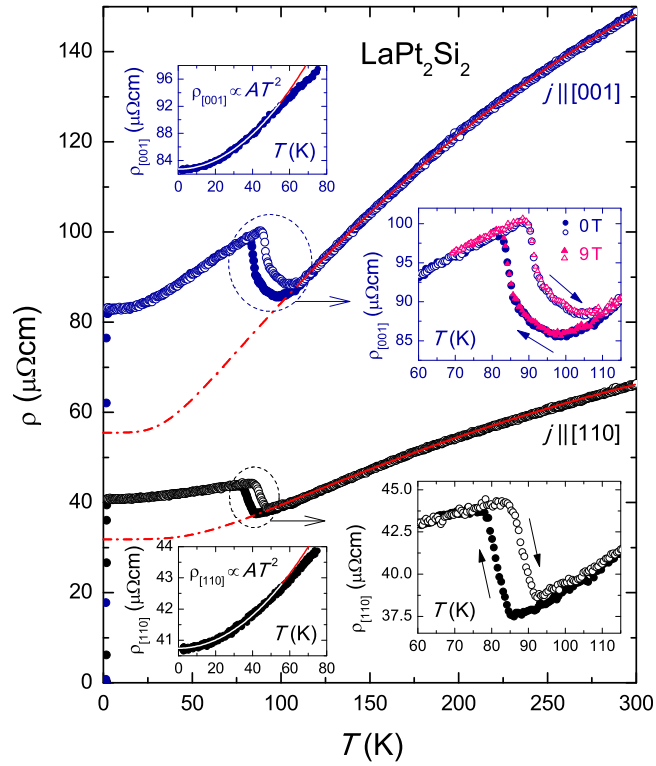


FIG. 8. Temperature dependence of the electrical resistivity $\rho(T)$ of $LaPt_2Si_2$ single crystal along the [110] axis (black symbols) and [001] axis (blue symbols). The solid curves superimposed onto the $\rho(T)$ data for $T > T_{CDW}$ are Bloch-Grüneisen-Mott fits [Eq. (3)]. Insets on the left side illustrates the low-$T$ dependence of $\rho$, just below the transition. The solid lines represent a fit according to the Fermi liquid type of behavior with parameters given in the text. Insets on the right side show the hysteretic behavior in $\rho(T)$ on an enlarged scale.

$\theta_R$ is the Debye temperature obtained from resistivity and $A_0$ is the electron-phonon coupling constant, and the third term stands for the scattering of the conduction electrons with electrons from a narrow $d$ band (so called $s$-$d$ Mott's type of scattering), $K$ being the Mott coefficient. The least-squares fit parameters are as follows: $\rho_0^{BGM} = 31.7$ $\mu\Omega$cm, $A_0 = 2.0$ $\mu\Omega$cm K, $\theta_R = 350$ K, $K = 2.1 \times 10^{-9}$ $\mu\Omega$cm K$^{-3}$ for $j \parallel$ [110] axis, and $\rho_0^{BGM} = 55.4$ $\mu\Omega$cm, $A_0 = 3.5$ $\mu\Omega$cm K, $\theta_R = 226$ K, and $K = 7.1 \times 10^{-9}$ $\mu\Omega$cm K$^{-3}$ for $j \parallel$ [001] axis. At low temperatures, $\rho(T)$ is dominated by a $T^2$ dependence, providing a good description up to 50 K for both crystallographic directions, which reflects the electron-electron scattering mechanism (see insets on the left side in Fig. 8). The fit of equation $\rho(T) = \rho_0 + AT^2$ to the data yields the residual resistivity $\rho_0 = 40.7$ $\mu\Omega$cm (82.7 $\mu\Omega$cm) and $A = 6.63 \times 10^{-4}$ $\mu\Omega$cm K$^{-2}$ ($3.23 \times 10^{-3}$ $\mu\Omega$cm K$^{-2}$) for $j \parallel$ [110] axis ($j \parallel$ [001] axis), respectively. The origin of the quadratic term can be confirmed by its relation to the density of electronic states at the Fermi level, expressed by the Kadowaki-Woods ratio $A/\gamma^2$ [31] expected to be $10^{-5}$ $\mu\Omega$cm mol$^2$ K$^2$ mJ$^{-2}$ [32–34]. From the values of $A$ coefficient obtained along the [110] and [001] axis, an estimated ratio $A/\gamma^2 = 1.1 \times 10^{-5}$ $\mu\Omega$cm mol$^2$ K$^2$ mJ$^{-2}$ for $j \parallel$ [110] and $A/\gamma^2 = 5.3 \times 10^{-5}$ $\mu\Omega$cm mol$^2$ K$^2$ mJ$^{-2}$ for $j \parallel$ [001],

using the low-$T$ $\gamma$ value. Despite the difference for the two current directions, which may be related to an anisotropy of the Fermi level, we obtain the ratio of the correct order of magnitude.

While the absolute values of $\rho_{[110]}$ and $\rho_{[001]}$ seem to indicate the anisotropic nature of the electrical conductivity, the $T$ dependencies are quite similar, i.e., show the similar values of the residual resistivity ratio (*RRR*) defined as $\rho(300\,\mathrm{K})/\rho(2\,\mathrm{K})$ and yields $RRR = 1.63$ for $j \parallel [110]$ and $RRR = 1.80$ for $j \parallel [001]$, respectively. The small *RRR* values along both crystallographic directions may in general indicate structural defects. However, resistivity in both directions jumps up when cooled through the transition at 85 K, the $\rho_0$ values expected from the high-$T$ part are significantly lower than the actual ones. Hence, we can estimate that *RRR* would reach at least the value of 2–3, if there was not for the increase of resistivity related to the structure phase transition. This change can be interpreted as a partial gapping of the density of states around the Fermi level. This gapping, related to the reduction of one-electron energies by means of additional lattice modulations, is one of fingerprints of a CDW state [35]. On the other hand, a similar driving force can be speculated at other types of structural phase transition, not excluding transition between two identical structure types.

In any case, the $\rho(T)$ data exhibit a metallic state even below the transition, indicating that the gapping in not complete, and part of electronic states at the Fermi level remains available for the formation of superconducting ground state. A rough estimate based on comparison of real and extrapolated $\rho_0$ values suggests that the pseudogap removes about 20% of $N(E_F)$ in the [110] direction and 30% in the [001] direction. As the resistivity can be measured during monotonous cooling and heating, it provides better insight into details of the transition, especially its hysteresis. The broad temperature hysteresis is evident as the loop between 77–92 K for $\rho_{[110]}$ and 83–110 K for $\rho_{[001]}$ demonstrates most likely a first-order character of the transition. In the insets on the right side in Fig. 8, we highlighted the temperature hysteretic behavior of the $\rho(T)$ in single-crystalline $LaPt_2Si_2$. Interestingly, we noticed that in the case of $\rho_{[001]}$ the hysteresis loop is wider and somewhat irregular compared to $\rho_{[110]}$. In particular, a precursor effect few kelvin above the critical temperature can be seen in resistivity both for the heating and cooling run for the [001] axis, even before the transition has any fingerprint in the lattice parameters, as one can see in Fig. 9. Electrical resistivity around the transition does not change in applied magnetic fields in the range of several tesla, proving that there is no relation of the structure phase transition with magnetic degrees freedom.

### D. Superconductivity

So as to observe possible superconductivity, a separate resistivity experiment was undertaken to cover the $T$ range 0.4–3 K using a $^3$He insert. In this case, both samples were measured separately. Magnetic field was applied perpendicular to the current direction. A sharp superconducting transition bringing resistivity to the zero value was indeed detected (see Fig. 10). The recorded actual values of critical temperature are for both directions slightly different, $T_c^{[110]} = 1.65$ K and

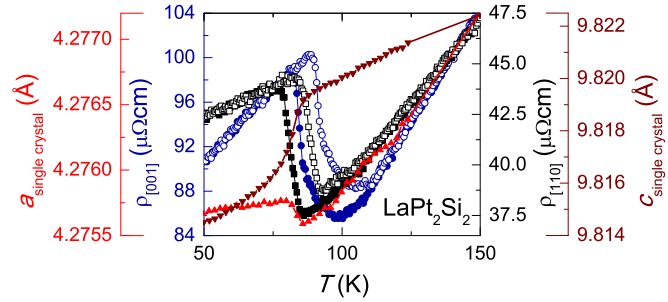


FIG. 9. Comparison of the temperature dependence of electrical resistivity (black: [110] axis, blue: [001] axis, full symbols: cooling, empty symbols: warming) with the temperature variations of lattice parameters.

$T_c^{[001]} = 1.5$ K (the $T_c$ are taken as $T$ where $\rho = 0$). At present it is not clear whether the small difference is an instrumental effect or perhaps due to an anisotropy of critical current value close to $T_c$.

The presence of superconductivity is a remarkable fact as archetypal CDW systems are not superconductors [35] as the two phenomena (CDW/SC) are competitive and detrimental to each other. In Figs. 10(a) and 10(b), we show the magnified view of the low-$T$ range together with effect of an applied magnetic field on the superconducting transition for both crystallographic directions. In both cases, $T_c$ gradually decreases with increasing field and already the field of 0.5 T pushes $T_c$ below 0.4 K.

In order to get some insight into the upper critical field values, $\mu_0 H_{c2}$, we used the resistivity data measured at a few selected magnetic field strengths of $\mu_0 H = 0$, 0.05, 0.1, and 0.2 T. The resulting upper critical field against temperature $\mu_0 H_{c2}(T)$ of $LaPt_2Si_2$ plotted both for $\mu_0 H \parallel [001]$ ($j \parallel [110]$) and $\mu_0 H \parallel [110]$ ($j \parallel [001]$) is shown in the main panel of Fig. 11. Similarly to the previous work [1], also our results of $\mu_0 H_{c2}(T)$ do not show the conventional saturating behavior, as they exhibit nearly linear increase with decreasing $T$. Moreover, in our case superconductivity vanishes faster and at lower magnetic fields than it was in the previous case. The unusual dependence, i.e., a small positive curvature in $\mu_0 H_{c2}(T)$ for $\mu_0 H \parallel [001]$ (see squares symbols in Fig. 11), however, remains. Such a behavior is not expected for a BCS superconductor with a weak coupling, described by the Werthamer, Helfand, Hohenberg (WHH) theory [36], accounting for the orbital pair breaking.

The dimensionless electron-phonon coupling constant, $\lambda_{\text{el-ph}}$ of $LaPt_2Si_2$ can be calculated via the McMillan formula [37]

$$T_c = \frac{\theta_D}{1.45} \exp\left[\frac{-1.04(1+\lambda_{\text{el-ph}})}{\lambda_{\text{el-ph}} - \mu^*(1+0.62\lambda_{\text{el-ph}})}\right] \quad (4)$$

putting the repulsive screened Coulomb pseudopotential $\mu^* = 0.13$, the Debye temperature deduced from the low-$T$ specific heat $\theta_D^{LT} = 217$ K and the value of the superconducting transition at zero field $T_c \simeq 1.6$ K, we obtained $\lambda_{\text{el-ph}} = 0.52$. This value is nearly the same as the one given in Ref. [1] and indicates that $LaPt_2Si_2$ locates rather on the border between the weak and an intermediate electron-phonon coupling regime.

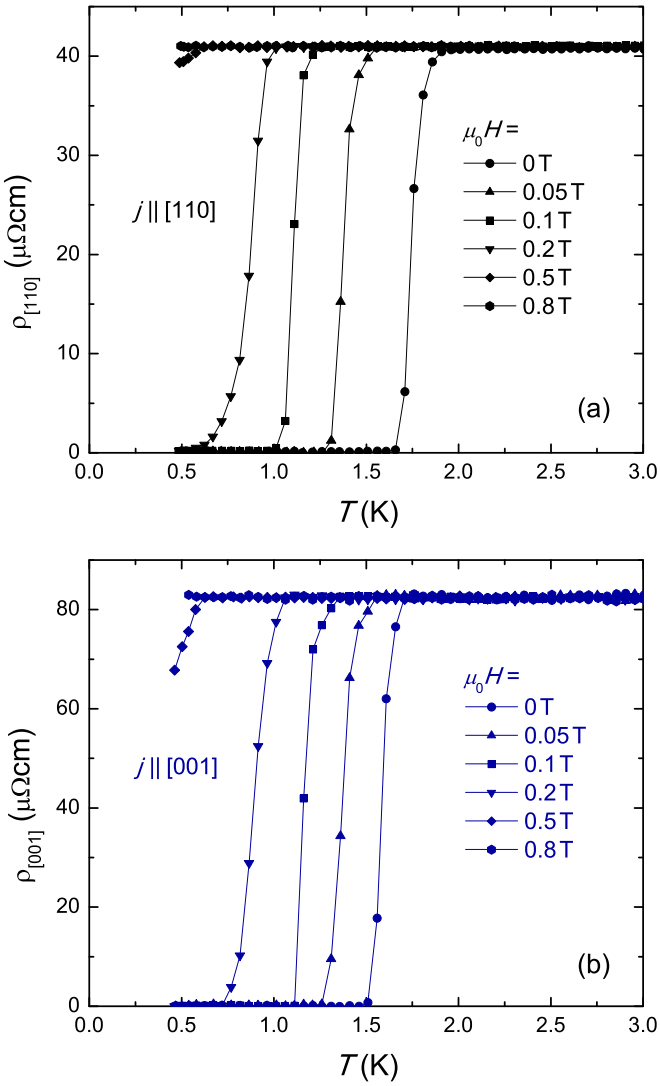


FIG. 10. Low-$T$ detail $\rho(T)$ in vicinity of the superconducting transition for both crystallographic directions of single-crystalline $LaPt_2Si_2$ in various applied magnetic fields.

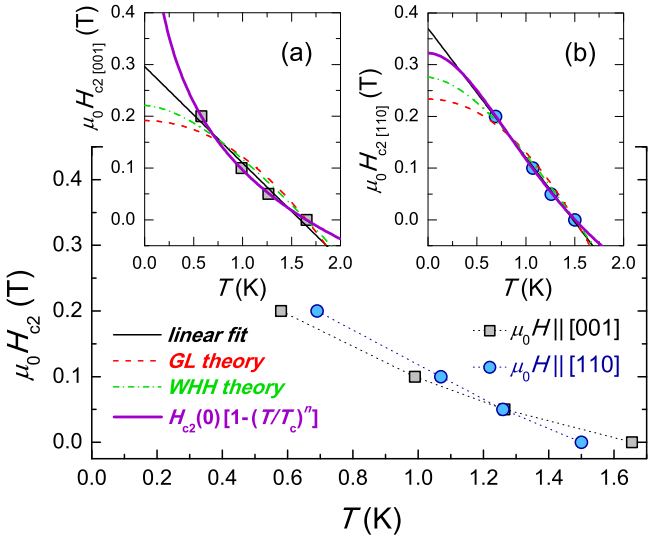


FIG. 11. Temperature variations of the upper critical field $\mu_0 H_{c2}(T)$ for $\mu_0 H \parallel [001]$ (squares) and $\mu_0 H \parallel [110]$ (circles) determined from the $\rho(T)$ measurements (dotted line is a guide to the eye). Insets (a) and (b) show $\mu_0 H_{c2}(T)$ for different crystallographic directions where the superimposed lines represent the fitting of the experimental data within the various models described in the text.

For the sake of clarity and in order to show the anomalous behavior of the upper critical field, we plotted in both insets in Fig. 11 $\mu_0 H_{c2}(T)$ for $\mu_0 H \parallel [001]$ (a) and $\mu_0 H \parallel [110]$ (b), together with theoretical analysis. The results are summarized in Table I.

In our analysis, we tried to reproduce the experimental $\mu_0 H_{c2}(T)$ data within the framework of two well-known models, namely WHH theory [36]

$$H_{c2}(0)^{\mathrm{WHH}} = -0.693 T_c \left(\frac{dH_{c2}}{dT}\right)_{T=T_c} \tag{5}$$

and the Ginzburg-Landau equation

$$H_{c2}(T)^{\mathrm{GL}} = H_{c2}(0)\frac{1-(T/T_c)^2}{1+(T/T_c)^2}. \tag{6}$$

As shown in the insets in Fig. 11, the data points of $\mu_0 H_{c2}(T)$ do not follow well the WHH and Ginzburg-Landau functions. This is well apparent in the inset (a) for $\mu_0 H \parallel [001]$, where $\mu_0 H_{c2}(T)$ shows a tendency for a faster than linear increase with decreasing $T$. Such a behavior is in contrast to both theoretical approaches, which predict the universal behavior of $\mu_0 H_{c2}(T)$ in superconductors with weak electron-phonon coupling. It strongly suggests that $LaPt_2Si_2$ is not the conventional BCS superconductor with an isotropic gap. Indeed, such an upward curvature of $\mu_0 H_{c2}(T)$ has been already reported for anisotropic gap [38,39] and multiband [40,41] superconductors. Even latest investigations by using muon spin rotation/relaxation ($\mu$SR) technique performed on polycrystalline material indicate a multigap superconductivity in $LaPt_2Si_2$ [42]. The analysis of the transverse field-$\mu$SR

TABLE I. Values of upper critical field at $T = 0$ K for both crystallographic axis of $LaPt_2Si_2$ estimated from the resistivity data at several constant magnetic fields by using different theoretical approaches. The last two columns show the values of the Ginzburg-Landau coherence length estimated from the Eq. (8).

| Theoretical approach | $\mu_0 H_{c2}(0)_{[001]}$ (T) | $\mu_0 H_{c2}(0)_{[110]}$ (T) | $\xi_{[001]}$ (Å) | $\xi_{[110]}$ (Å) |
|---|---|---|---|---|
| linear extrapolation | 0.2964 | 0.3692 | 333.1 | 298.5 |
| Ginzburg-Landau equation | 0.1921 | 0.2333 | 413.8 | 375.5 |
| WHH formula | 0.2211 | 0.2749 | 385.7 | 345.9 |
| $H_{c2}(0)[1-(T/T_c)^n]$ | 1.1965 ($n = 0.32$) | 0.3219 ($n = 1.87$) | | |

spectra in the superconducting state suggests that the Fermi surface may contains two gaps of different magnitude rather than an isotropic gap expected for a conventional superconductor. From other reasons we might consider an inhomogeneity of superconductivity and multiple superconducting phases [43]. However, the sharp transitions in $\rho(T)$ and $C_p(T)$ [1] in zero field seem to exclude this option, being corroborated by the single-phase character seen in XRD and EDX analysis. Other reasons, related to presence of magnetic impurities or spin fluctuations near $T_c$ [44] can be refuted as $LaPt_2Si_2$ is a nonmagnetic. Another possible reason for the unconventional behavior of $\mu_0 H_{c2}(T)$ could be the presence of the strong anisotropy in transport properties and also different values of $T_c$ for the [110] and [001] axis, incompatible with any spherical gap model.

A satisfactory description of experimental data was obtained using a phenomenological function with an adjustable power-law coefficient

$$H_{c2}(T) = H_{c2}(0)[1 - (T/T_c)^n] \tag{7}$$

with parameters given in the Table I. It should also be noted that the values of $\mu_0 H_{c2}(0)$ for $\mu_0 H \parallel [001]$ and $\mu_0 H \parallel [110]$ obtained from the linear extrapolation and also by using WHH and Ginzburg-Landau models in our case are smaller in comparison to earlier results of upper critical field at $T = 0$ K reported for the single-crystalline [1] as well as the polycrystalline [45] samples of $LaPt_2Si_2$. Irrespective of the model used, we see that the $\mu_0 H_{c2}(0)$ values are lower for field along [001] axis. This fact can be related to the higher normal-state electrical conductivity in the basal plane, important for the orbital pair-breaking induced by field along [001] axis.

Finally, from the knowledge of the value of $\mu_0 H_{c2}(0)$ it is now possible to determine the Ginzburg-Landau coherence length $\xi$ from the equation

$$\xi = \sqrt{\frac{\phi_0}{2\pi H_{c2}(0)}}, \tag{8}$$

where $\phi_0 = 2.068 \times 10^{-15}$ Wb is the magnetic flux quantum. The estimated values of $\xi$ regarding to $\mu_0 H \parallel [001]$ and [110], and for $\mu_0 H_{c2}(0)$ obtained from different models are presented in Table I.

### E. Thermoelectric power and thermal conductivity

The results of temperature-dependent thermoelectric power measurements $S(T)$, with the temperature gradient $\Delta T$ applied along the [110] and [001] axes, performed under cooling and warming conditions, are summarized in Fig. 12. One can compare the results with those obtained recently on polycrystalline $LaPt_2Si_2$ by Gupta *et al.* [46]. As seen, the $LaPt_2Si_2$ single crystal exhibits a large anisotropy in $S(T)$ both as to the absolute values and the sign of the Seebeck coefficient. Despite different values at $T = 300$ K ($-0.2\ \mu$V K$^{-1}$ for $\Delta T \parallel [110]$ and $-4.8\ \mu$V K$^{-1}$ for $\Delta T \parallel [001]$) the magnitude of $S$ is generally small, what characterizes ordinary metals without enhanced electronic correlations at the Fermi surface. In the high-$T$ range, both $S_{[110]}$ and $S_{[001]}$ are weakly

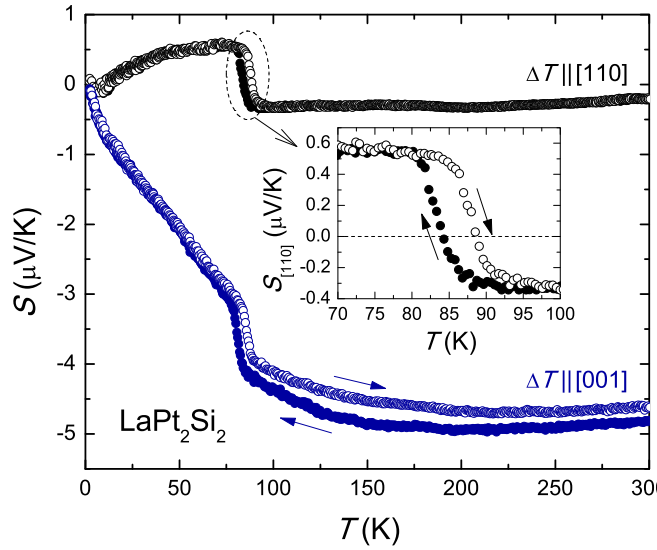


FIG. 12. Temperature dependence of the thermoelectric power $S(T)$ of $LaPt_2Si_2$ single crystal along the [110] axis (black symbols) and [001] axis (blue symbols). Inset shows the presence of thermal hysteresis near $T_{CDW}$, which is clearly visible for $\Delta T \parallel [110]$, corroborating the first-order nature of the phase transition.

temperature-dependent with negative values, indicating that electronlike carriers dominate in thermoelectric power. Note that such a weakly or sublinear temperature-dependent behavior in $S(T)$ usually indicates a dominant role of the diffusion component in the carriers transport, as it is envisaged in the case of metallic systems. In common with the electrical resistivity data, also $S(T)$ was found to undergo the CDW transition in the vicinity of 85 K. A rapid change in the slope of $S(T)$ is clearly evident at $T_{CDW}$ on cooling and warming processes for both crystallographic directions. Except for the hysteresis at the transition, $S_{[110]}$ is fully reversible. However, $S_{[001]}$ displayed an irreversibility between cooling and warming cycles on the high-$T$ side, which may be attributed to straining at the structural transition, either leaving microcracks or affecting the contacts, both slightly affecting the geometry of the experimental setup. As shown in the inset of Fig. 12, a well-defined temperature hysteresis of 4.5 K in $S_{[110]}$ appears around $T_{CDW}$. An interesting feature is the sudden change of sign in $S_{[110]}$, which indicates that both type of carriers, electrons and holes are involved in the thermal transport. The electronic structure is apparently changed abruptly, modifying the electron-hole asymmetry, or perhaps creating a new hole Fermi surface at low temperatures. Below $T_{CDW}$, both $S_{[110]}$ and $S_{[001]}$ vanish nearly linearly with temperature $|S(T) \to 0|_{T \to 0}$, as expected for metals. This picture seems to match the low-$T$ resistivity data, which follow the Fermi liquid relation of $\rho(T) \sim AT^2$, thereby confirming a metal-metal character of the transition and suggesting only partial opening of a gap at the Fermi surface below $T_{CDW}$.

The temperature dependences of total thermal conductivity $\kappa(T)$ of $LaPt_2Si_2$ for $\Delta T$ along [110] and [001] axis during cooling and warming (circle symbols) are shown in the panels (a) and (b) in Fig. 13. One can see a pronounced anisotropy in heat conduction as well as an anomaly near $T_{CDW}$. The absolute value of total $\kappa_{[110]}$ is higher than $\kappa_{[001]}$ over the

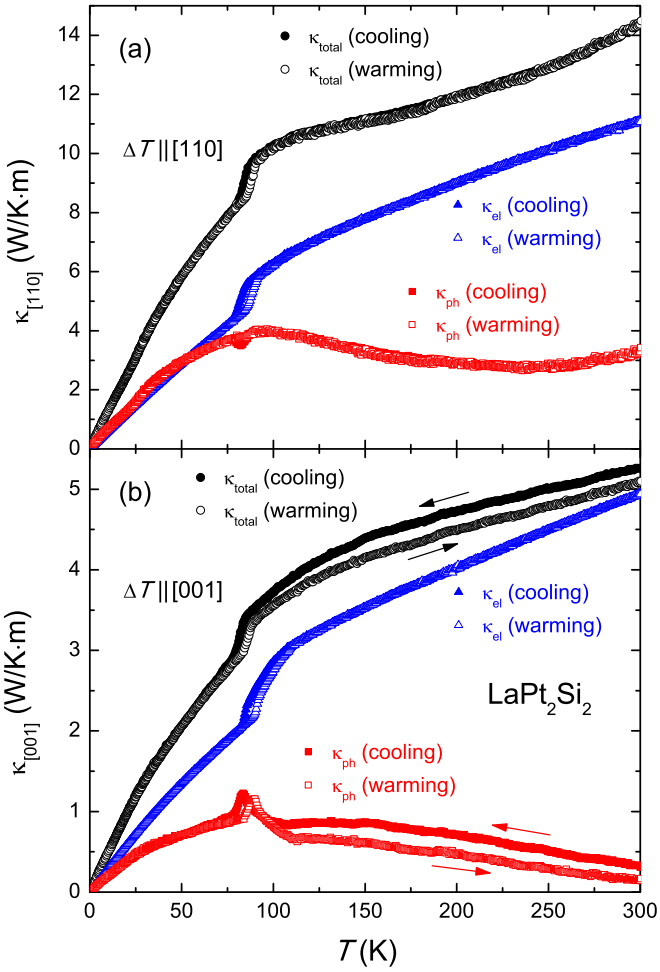


FIG. 13. Temperature dependencies of the total measured thermal conductivity $\kappa(T)$ of single-crystalline $LaPt_2Si_2$ along the [110] axis (a) and [001] axis (b), together with an electronic $\kappa_{el}(T)$ contribution estimated via Wiedemann-Franz law as described in the text, as well as the lattice $\kappa_{ph}(T)$ contribution.

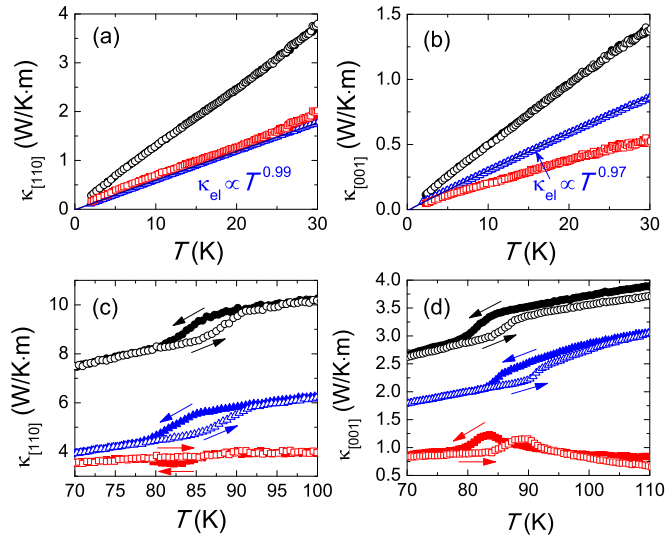


FIG. 14. (a) and (b) show the expanded view of $\kappa(T)$ (circles), $\kappa_{el}(T)$ (triangles), and $\kappa_{ph}(T)$ (squares) dependencies at low temperatures, with the various temperature relations for respective contributions as discussed in the text. (c) and (d) present the temperature hysteretic behavior near $T_{CDW}$ in detail.

whole investigated $T$ range, with the ration reaching at $T =$ 300 K almost the factor of 3. In rare earth compounds the $f$-electron scattering mechanism plays a major role reducing the thermal conductivity, providing a source of anisotropy. Since the La has no $f$ electrons, such a large reduction in $\kappa(T)$ depending on the crystallographic direction is rather unusual. The low thermal conductivity along [001] axis can be related to the high electrical resistivity for $j \parallel [001]$, but can be also due to the heat conductivity of crystal lattice. In general, the thermal conductivity strongly depends on the degree of crystallinity of the material and represents a sensitive probe for any lattice instability.

In metals, the thermal conductivity is a sum of two contributions, coming from electrons and phonons, respectively. Knowing $\rho(T)$, we can specify the electronic contribution to thermal conductivity $\kappa_{el}(T)$ assuming the Wiedemann-Franz law: $\kappa_{el}(T) = L_0 T/\rho(T)$, where $L_0 = \pi^2 k_B^2/3|e| = 2.45 \times 10^{-8}$ W Ω K$^{-2}$ is the temperature-independent Lorenz number. $\kappa_{el}(T)$ can be used to estimate, using experimental $\kappa(T)$, the lattice contribution: $\kappa_{ph}(T) = \kappa(T) - \kappa_{el}(T)$. Both components are also plotted in Fig. 13 as triangle symbols for $\kappa_{el}$ and square symbols for $\kappa_{ph}$. As one can see in Fig. 13, $\kappa_{el}(T)$ dominates over $\kappa_{ph}(T)$, indicating that heat transport in $LaPt_2Si_2$ is evidently governed by the charge carriers. This observation matches with results obtained for a polycrystalline sample [46] and correlates well with a metallic nature of conductivity dominated by the free electron gas as expected in the case of simple metals. On the low-$T$ side, below 30 K, $\kappa_{el}(T)$ for $\Delta T \parallel$ [110] and [001] axis show a linear dependence on $T$ [see panels (a) and (b) in Fig. 14]. This indicates a dominance of elastic electron scattering on static lattice imperfections, which is the most common and efficient process of electron scattering at low temperatures in metals. The lattice contribution, $\kappa_{ph}(T)$, which deviates from the expected $\kappa_{ph} \propto T^3$ dependence of phonons, showing a nearly linear $T$-dependent behavior both along the [110] and [001] axis. This is rather uncommon for a nonmagnetic metal. In magnetic materials, such a strong deviation from a power-law behavior in $\kappa_{ph}$ is caused by the resonant scattering of phonons through excitations of the spins on the magnetic ions and also scattering mechanism due to spin ordering (magnons). In a nonmagnetic material as $LaPt_2Si_2$ single crystal, we can speculate about anharmonicity as a possible reason [47], which can be due to modulation of atomic positions in crystal lattice, i.e., the CDW effect.

In the vicinity of $T = 85$ K, $\kappa(T)$, $\kappa_{el}(T)$, and $\kappa_{ph}(T)$ along [110] and [001] axis demonstrate the characteristic features attributed to the CDW transition. In the panels (c) and (d) in Fig. 14, we highlighted the temperature hysteretic behavior near $T_{CDW}$. For $\kappa_{[110]}$, as well as for its components the full hysteresis loops are clearly observed. $\kappa_{[001]}$, similarly as $S_{[001]}$ exhibits an irreversibility between the cooling and warming mode above $T_{CDW}$. Considering that $\kappa(T)$ was measured simultaneously with $S(T)$ we see here also a fingerprint of opening microcracks, opened perpendicular to [001] direction, affecting thus the [001] axis transport.

## IV. CONCLUSIONS AND SUMMARY

A single crystal of $LaPt_2Si_2$ grown by the Czochralski method, characterized by powder and single crystal x-ray diffraction and EDX analysis, was used to investigate the structure, thermodynamic, thermal and electron transport properties and their anisotropy. The structure study confirmed noncentrosymmetric tetragonal structure of the $CaBe_2Ge_2$-type, undergoing a structural phase transition of the first-order type at $T = 85$ K, which is suggestive of a low-$T$ CDW state. The satellites corresponding to the wave vector $q \approx (0.36, 0, 0)$ could be observed at higher temperatures, growing from $T = 175$ K and declining (or shifting from observable part of reciprocal space) below 85 K. The lattice parameters are modified, the reduced $c$ and enhanced $a$ largely compensate each other so that the volume effect is very small. The first-order transition strongly affects electron and thermal transport properties, interpreted as a formation of a pseudo gap, so it is quite likely that the driving force of the transition is in the electron sub-system.

Detailed studies of $C_p(T)$, $\rho(T)$, $S(T)$, and $\kappa(T)$ identified a substantial temperature hysteresis of the transition, and a precursor effect several degrees kelvin above the transition. Metallic behavior at low temperatures, which means only partial gapping of the Fermi surface, allows to develop a superconducting ground state, proved to be an intrinsic property. The superconductivity itself exhibits certain unconventional features, not compatible with the common weak coupling BCS model. Namely, the field dependence of the upper critical field deviates in both crystallographic directions from the conventional WHH or Ginzburg-Landau behavior. Furthermore, from our $\rho(T)$, $S(T)$, and $\kappa(T)$ measurements performed along the [110] and [001] axis, we arrived at the important conclusion that the electron and thermal transport shows strongly anisotropic properties, which may also affect $\mu_0 H_{c2}(T)$.

The Sommerfeld coefficient $\gamma = 7.8$ mJ mol$^{-1}$ K$^{-2}$ and Debye temperature of 205 K could be derived at low temperatures, but the $C_p$ has a strongly non-Debye like $T$ dependence, which can be ascribed to a low-energy Einstein mode.

In future, it would be interesting to compare the parameters of the structure phase transition with analogous compounds with other rare earths, which can provide a fine tuning of the lattice by changing the rare earth size, and which can also include magnetic degrees of freedom and their interplay with modifications of underlying electronic structure. Naturally also in such studies single crystals are an important prerequisite.

## ACKNOWLEDGMENTS

The work was supported by the project 19-00925S of the Czech Science Foundation and by the Materials Growth and Measurement Laboratory (MGML, https://mgml.eu). M.F. acknowledges support from the project SOLID21 through Grant No. CZ.02.1.01/0.0/0.0/16_019/0000760. The work was also supported within the project NanoCent-Nanomaterials center for advanced applications, Project No. CZ.02.1.01/0.0/0.0/15_003/0000485, financed by the ERDF.

[1] R. Gupta, S. K. Dhar, A. Thamizhavel, K. P. Rajeev, and Z. Hossain, J. Phys.: Condens. Matter **29**, 255601 (2017).
[2] A. M. Gabovich, A. I. Voitenko, J. F. Annett, and M. Ausloos, Supercond. Sci. Technol. **14**, R1 (2001).
[3] T. Kiss, T. Yokoya, A. Chainani, S. Shin, T. Hanaguri, M. Nohara, and H. Takagi, Nat. Phys. **3**, 720 (2007).
[4] K. Machida and M. Kato, Phys. Rev. B **36**, 854 (1987).
[5] R. E. Peierls, *Quantum Theory of Solids* (Oxford University Press, London, 1955), p. 108.
[6] H. Fröhlich, Proc. R. Soc. London A **223**, 296 (1954).
[7] G. Grüner, Rev. Mod. Phys. **60**, 1129 (1988).
[8] K. D. Myers, S. L. Bud'ko, I. R. Fisher, Z. Islam, H. Kleinke, A. H. Lacerda, and P. C. Canfield, J. Magn. Magn. Mater. **205**, 27 (1999).
[9] C. Song, J. Park, J. Koo, K.-B. Lee, J. Y. Rhee, S. L. Bud'ko, P. C. Canfield, B. N. Harmon, and A. I. Goldman, Phys. Rev. B **68**, 035113 (2003).
[10] C. S. Lue, Y. F. Tao, K. M. Sivakumar, and Y. K. Kuo, J. Phys.: Condens. Matter **19**, 406230 (2007).
[11] B. Becker, N. G. Patil, S. Ramakrishnan, A. A. Menovsky, G. J. Nieuwenhuys, J. A. Mydosh, M. Kohgi, and K. Iwasa, Phys. Rev. B **59**, 7266 (1999).
[12] Y.-K. Kuo, C. S. Lue, F. H. Hsu, H. H. Li, and H. D. Yang, Phys. Rev. B **64**, 125124 (2001).
[13] Y. Singh, D. Pal, S. Ramakrishnan, A. M. Awasthi, and S. K. Malik, Phys. Rev. B **71**, 045109 (2005).
[14] Y.-K. Kuo, K. M. Sivakumar, T. H. Su, and C. S. Lue, Phys. Rev. B **74**, 045115 (2006).
[15] C. S. Lue, Y.-K. Kuo, F. H. Hsu, H. H. Li, H. D. Yang, P. S. Fodor, and L. E. Wenger, Phys. Rev. B **66**, 033101 (2002).
[16] N. Yamamoto, R. Kondo, H. Maeda, and Y. Nogami, J. Phys. Soc. Jpn. **82**, 123701 (2013).
[17] S. Shimomura, C. Hayashi, G. Asaka, N. Wakabayashi, M. Mizumaki, and H. Onodera, Phys. Rev. Lett. **102**, 076404 (2009).
[18] A. Wolfel, L. Li, S. Shimomura, H. Onodera, and S. van Smaalen, Phys. Rev. B **82**, 054120 (2010).
[19] S. Shimomura, C. Hayashi, N. Hanasaki, K. Ohnuma, Y. Kobayashi, H. Nakao, M. Mizumaki, and H. Onodera, Phys. Rev. B **93**, 165108 (2016).
[20] G. H. Lander, E. S. Fisher, and S. D. Bader, Adv. Phys. **43**, 1 (1994).
[21] D. Graf, R. Stillwell, T. P. Murphy, J. H. Park, M. Kano, E. C. Palm, P. Schlottmann, J. Bourg, K. N. Collar, J. Cooley, J. Lashley, J. Willit, and S. W. Tozer, Phys. Rev. B **80**, 241101(R) (2009).
[22] I. Hase and T. Yanagisawa, Physica C **484**, 59 (2013).
[23] S. Kim, K. Kim, and B. I. Min, Sci. Rep. **5**, 15052 (2015).
[24] Y. Nagano, N. Araoka, A. Mitsuda, H. Yayama, H. Wada, M. Ichihara, M. Isobe, and Y. Ueda, J. Phys. Soc. Jpn. **82**, 064715 (2013).

[25] D. Kriegner, Z. Matěj, R. Kužel, and V. Holý, J. Appl. Crystallography **48**, 613 (2015).
[26] J. Rodriguez-Carvajal, Physica B (Amsterdam) **192**, 55 (1993).
[27] S. Mašková, A. M. Adamska, L. Havela, N.-T. H. Kim-Ngan, J. Przewoźnik, S. Daniš, K. Kothapalli, A. V. Kolomiets, S. Heathman, H. Nakotte, and H. Bordallo, J. Alloys Comp. **522**, 130 (2012).
[28] W. N. Lawless, Phys. Rev. B **14**, 134 (1976).
[29] A. Tari, *The Specific Heat of Master at Low Temperatures* (Imperial College Press, London, 2003), pp. 23–38.
[30] N. F. Mott, H. Jones, *The Theory of the Properties of Metals and Alloys* (Oxford University Press, London, 1958).
[31] K. Kadowaki and S. B. Woods, Solid State Commun. **58**, 507 (1986).
[32] K. Yamada and K. Yosida, Prog. Theor. Phys. **76**, 621 (1986).
[33] P. Coleman, Phys. Rev. Lett. **59**, 1026 (1987).
[34] T. C. Li and J. W. Rasul, Phys. Rev. B **39**, 4630 (1989).
[35] R. E. Thorne, Phys. Today **49**(5), 42 (1996).
[36] N. R. Werthamer, E. Helfand, and P. C. Hohenberg, Phys. Rev. **147**, 295 (1966).
[37] W. L. McMillan, Phys. Rev. **167**, 331 (1968).
[38] S. V. Shulga, S. L. Drechsler, G. Fuchs, K. H. Müller, K. Winzer, M. Heinecke, and K. Krug, Phys. Rev. Lett. **80**, 1730 (1998).
[39] T. Tamegai, Y. Nakajima, T. Nakagawa, G. J. Li, and H. Harima, J. Phys.: Conf. Ser. **150**, 052264 (2009).
[40] L. Lyard, P. Samuely, P. Szabo, T. Klein, C. Marcenat, L. Paulius, K. H. P. Kim, C. U. Jung, H. S. Lee, B. Kang, S. Choi, S. I. Lee, J. Marcus, S. Blanchard, A. G. M. Jansen, U. Welp, G. Karapetrov, and W. K. Kwok, Phys. Rev. B **66**, 180502(R) (2002).
[41] F. Hunte, J. Jaroszynski, A. Gurevich, D. C. Larbalestier, R. Jin, A. S. Sefat, M. A. McGuire, B. C. Sales, D. K. Christen, and D. Mandrus, Nature (London) **453**, 903 (2008).
[42] D. Das, R. Gupta, A. Bhattacharyya, P. K. Biswas, D. T. Adroja, and Z. Hossain, Phys. Rev. B **97**, 184509 (2018).
[43] M. Falkowski, A. Kowalczyk, A. M. Strydom, M. Reiffers, and T. Toliński, J. Low Temp. Phys. **189**, 120 (2017).
[44] M. Cyrot, Rep. Prog. Phys. **36**, 103 (1973).
[45] R. Gupta, U. B. Paramanik, S. Ramakrishnan, K. P. Rajeev, and Z. Hossain, J. Phys.: Condens. Matter **28**, 195702 (2016).
[46] R. Gupta, K. P. Rajeev, and Z. Hossain, J. Phys.: Condens. Matter **30**, 475603 (2018).
[47] C. Chang and L.-D. Zhao, Mater. Today Phys. **4**, 50 (2018).